IEEE Access
Multidisciplinary | Rapid Review | Open Access Journal

Received November 27, 2017, accepted January 2, 2018, date of publication January 8, 2018, date of current version February 28, 2018.

Digital Object Identifier 10.1109/ACCESS.2018.2790933

Time-Frequency Scheduling and Power Optimization for Reliable Multiple UAV Communications

ZHEN XUE[1], JINLONG WANG[1], (Senior Member, IEEE), QINGJIANG SHI[2], GUORU DING[1], (Senior Member, IEEE), AND QIHUI WU[2], (Senior Member, IEEE)

[1]College of Communications Engineering, Army Engineering University of PLA, Nanjing 210007, China
[2]College of Electronic and Information Engineering, Nanjing University of Aeronautics and Astronautics, Nanjing 210016, China

Corresponding author: Guoru Ding (dr.guoru.ding@ieee.org)

This work was supported in part by the Natural Science Foundation of Jiangsu Province under Grant BK20150717, in part by the National Natural Science Foundation of China under Grant 61501510 and Grant 61631020, and in part by China Post-Doctoral Science Funded Project under Grant 2016M590398.

ABSTRACT Unmanned aerial vehicle (UAV) communication has gained increasing interests from the industry and academia as UAV has a variety of emerging applications, such as aerial sensors, flying base stations, and mobile relays. Generally, UAVs are manipulated by remote ground control center. Thus one critical issue is that UAVs must correctly receive the control signal before following the instructions. However, the control signal quality at UAV receivers is very susceptible due to the variation of channel conditions and the effect of adjacent channel interference. To tackle these challenges, this paper investigates the issue of how to simultaneously ensure the reliability of the remote control signal for multiple UAVs. The problem is formulated as a mixed-integer programming with the goal of maximizing the minimum signal to interference-plus-noise ratio of all UAVs by jointly scheduling the time–frequency resource blocks and optimizing the power allocation. To make the problem tractable, we perform equivalent transformations via leveraging the inherent property of the formulated problem. Next, based on the decoupled constraints on different variables, we propose a low complexity block coordinate descent-based method. Furthermore, to offer better system performance, we leverage the smooth approximation theory and develop a gradient projection-based method. Finally, extensive simulation results demonstrate the effectiveness of the proposed methods under various parameter configurations.

INDEX TERMS Unmanned aerial vehicle communications, adjacent channel interference, time-frequency scheduling, power optimization.

I. INTRODUCTION

A. BACKGROUND AND MOTIVATION

Unmanned aerial vehicles (UAVs) aided wireless communication is a promising approach complementing to the terrestrial mobile communication systems that are largely dependent on the fixed infrastructure. Due to its flexible deployment and stable maneuverability, the UAV platform equipped with machine-type communications (MTCs) devices can support a variety of communication systems [1]–[3]. On one hand, UAVs could act as flying base stations (BSs) to serve ground targets when the terrestrial infrastructure is damaged by natural disasters or overloaded in hotpot areas; on the other hand, the UAV aided mobile relaying system can offer connectivity opportunities for distant communication nodes and promote the system performance by leveraging its mobility [4], [5].

To effectively accomplish the above mentioned tasks, UAVs require specific high-level coordination support, especially in highly dynamic, heterogeneous environments [2]. Multiple-UAV operations introduces many non-trivial problems. One critical technical challenge is that the safety and stability of UAV communications require the robustness of control signals, whereas the quality of the control signal is sensitive to channel variation and interference. Another challenge is that the available resources for communications are usually limited, which may aggravate the potential mutual interference. Those observations motivate us to investigate the issue that

how to promote the reliability of control signals received by UAVs in this paper.

B. RELATED WORK AND CONTRIBUTION

Recently, extensive studies have been devoted to the UAV-based wireless communications; those efforts mainly focus on a number of technical issues such as modeling air-ground channel [6], [7], performance analysis [4], [8], resource management [9]–[11], UAV deployment and trajectory optimization [12]–[15].

Resource optimization provides effective ways to improve the system performance of the UAV-aided wireless communications. Zhang and Zhang [9] have investigated the three-dimensional (3D) drone small cells (DSCs) network sharing the underlying spectrum with the cellular networks, and considered to maximize the DSCs network throughput while satisfying the cellular network efficiency constraint. By considering the UAVs' endurance time, the work in [10] studied UAVs as flying BSs, and proposed a framework for optimizing the data service delivered to the users. The work in [11] investigated the problem of synthesizing communication networks of UAVs, which considered to maximize the connectivity subject to the cost of operation in the presence of resource constraints. In [13], the throughput of a point-to-point mobile relaying system is maximized by optimizing the source/relay transmit power and the trajectory of the relaying UAV. Due to that the resource scheduling problems for multiple UAVs usually involve the difficult discrete variable optimization, there are few related studies. The work in [15] jointly considered multiuser scheduling, user association, UAVs' transmit power and trajectory, which aimed to achieve the fair performance among users. In [15], to handle the discrete UAV scheduling problem, the discrete variables are directly relaxed into continuous optimization variables without considering their properties, which can not be applied to this work, and we explain the peculiar phenomenon in Section V.

However, none of those prior studies have investigated multiple UAVs coordinations for the reliable control signal reception. Many existing works explicitly or implicitly assume that the UAV can be perfectly controlled by the control center. Nevertheless, in practice the control signal reception of UAV is not only affected by the link quality of the communication channel, but also very susceptible to the potential interference. Hence, the maintenance of control links between the control center and UAVs is an important but tough job. The situation could be more challenging when the resource such as spectrum resource and transmit power are constrained.

In this paper, we focus on a multiple UAVs enabled uplink communication system, where the control center connects to a ground base station, which is referred to as the control BS or BS hereinafter. To effectively carry out the target missions, the UAVs have to correctly receive the control signal and follow the instructions wherein to adjust the response, but the number of available frequency bands is not sufficient to schedule all UAVs. In addition, due to the hardware limitations, UAVs that are occupying adjacent channels simultaneously would suffer from the interference leaked from other channels. This phenomenon can be rather serious when the near-far effect exists between UAVs. To tackle these challenges inherent in the reliable control signal reception of multiple UAVs, this paper makes the following contributions:

- We formulate a novel max-min-fairness problem for optimizing the quality of the control signal received at UAVs under the effect of adjacent channel interference. This formulation can fairly guarantee the reliable control signal reception of UAVs by jointly considering the time-frequency scheduling of UAVs and the transmit power allocation of the BS. However, this problem is an intractable Mixed-Integer Nonlinear Program (MINLP).
- We perform transformation for the formulated challenging optimization problem. By introducing the definition of the resource blocks assignment matrix, we derive a more tractable formulation. To further simplify the form of the problem, we leverage the rank-one property to reduce the scale of the optimization variables. In addition, we decouple the variables from the coupling constraints by exploiting the property of the objective function.
- We develop two algorithms for the maximization of the lowest signal-to-interference plus noise ratio (SINR) at UAVs. The first one is the low complexity, block coordinate descent (BCD) based method, which is designed based on the property that the constraints are separable across the variables. The second algorithm is proposed to approximate the best system performance, which is based on the concept of smooth approximation and gradient projection.
- We provide in-depth simulations under various parameter configurations. The results clearly show the convergence behaviors of the proposed methods, the effect on the system performance of various parameters, and the insights of a typical example. Moreover, the comparison results demonstrate the superior performance of the proposed methods.

C. ORGANIZATION AND NOTATIONS

The rest of this paper is organized as follows. In the next section, we describe the system model and state the problem formulation. The problem transformation is presented in III. Section IV proposes a block coordinated descend based method. The smooth approximation and the gradient projection based method are discussed in Section V. Simulation results are provided in Section VI, and the conclusions are drawn in Section VII.

Notations: Scalars, vectors and matrices are respectively denoted by lower case, boldface lower case and boldface upper case letters. For a square matrix $\mathbf{A}$, $\mathbf{A}^T$, $\mathbf{A}^{-1}$ and $\lambda_{\max}(\mathbf{A})$ denote its transpose, inverse, and the maximum eigenvalue, respectively. $\mathbb{R}^{M\times N}$ denotes the space of the

$M \times N$-dimensional real-valued matrix and $\mathbf{E}$ denotes the matrix with 1 in all entries.

II. SYSTEM MODEL AND PROBLEM STATEMENT

As shown in Fig. 1, we consider the uplink scenario where a number of UAVs are controlled by a control BS to carry out certain tasks, and the control BS needs to frequently send control messages to the UAVs. However, the mutual interference occurs between different UAVs on adjacent channels. The adjacent channel interference (ACI) may become more serious when UAVs have relatively large differences with respect to the distance to the BS. For example, two UAVs u_1 and u_2 receive their control signals on adjacent channels, $d_{u_1,bs}$ and $d_{u_2,bs}$ are their distance to the BS. If $d_{u_1,bs} \gg d_{u_2,bs}$, due to the ACI, the high power signal transmitted to UAV u_1 would leak into the channel of UAV u_2 and block the communication between UAV u_2 and the BS.

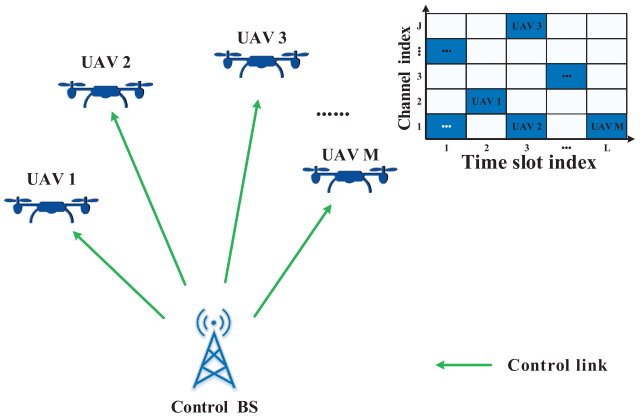

FIGURE 1. Scenario illustration of multiple UAVs enabled uplink control system.

Let $\mathcal{M} \triangleq \{1, ..., M\}$ denote the set of UAVs, $\mathcal{N} \triangleq \{1, ..., N\}$ and $\mathcal{J} \triangleq \{1, ..., J\}$ are the set of available frequency bands and time slots, respectively, thus the number of available resource blocks (RBs) of time-frequency is NJ. The time slot length is chosen sufficiently small such that the UAV's location can be regarded as constant within each slot, while different time slots represent the communication window of different periods. UAVs periodically send back their information, and a central processing unit at the control BS has the knowledge of all the UAVs' state information, including their flying 3D coordinates and channel state information (CSI). The objective of the BS is to alleviate the ACI effect and improve the quality of control signal for all the UAVs, by assigning UAVs the proper resource blocks and optimizing the transmission power of the BS to each UAV. For this purpose, an optimization framework is required. In the sequel, before stating the problem formulation, we first present the AG channel model, and then give an explicit definition to quantify the ACI effect.

A. AIR-GROUND CHANNEL MODELING

According to [6] and [7], the air-ground (AG) communication link between a UAV and BS is mainly dominated by the line-of-sight (LoS) and non-line-of-sight (NLoS) occurrence probabilities. One typical modeling for the LoS probability between UAV k and the BS at the j-th slot is given by [4], [6], [7]:

$$\Pr_{LoS}^{k,j} = \frac{1}{1 + Ce^{\left[-B\left(\theta_k^j - C\right)\right]}} \tag{1}$$

where the constants B and C are dependent on the environment type (such as rural, urban, or dense urban), and θ_k^j is the elevation angle from the BS' view towards UAV k at the j-th slot. Definitely, $\theta_k^j = \frac{180}{\pi} \times \sin^{-1}\left(\frac{h_k^j}{d_{k,bs}^j}\right)$, where $d_{k,bs}^j = \sqrt{\left(x_k^j - x_{bs}\right)^2 + \left(y_k^j - y_{bs}^j\right)^2 + \left(h_k^j\right)^2}$ is distance between the coordinate of UAV k $\left(x_k^j, y_k^j, h_k^j\right)$ and the BS $(x_{bs}, y_{bs}, 0)$ at slot j. Clearly, the probability of NLoS link is $\Pr_{NLoS}^{k,j} = 1 - \Pr_{LoS}^{k,j}$.

Based on the free space propagation model [16], the path loss for LoS and NLoS links between UAV k and the BS at slot j is written as

$$PL_{k,bs}^j = \begin{cases} 20\lg(F + f_k^j) + 20\lg(d_{k,bs}^j) + 32.4 \\ \qquad + \eta_{LoS}, & \text{LoS link}, \\ 20\lg(F + f_k^j) + 20\lg(d_{k,bs}^j) + 32.4 \\ \qquad + \eta_{NLoS}, & \text{NLoS link}, \end{cases} \tag{2}$$

where F is the baseline carrier frequency, $f_k^j \in \{\triangle f_1, \ldots, \triangle f_N\}$ denotes the interval between the channel frequency that UAV k occupies at the j-th slot and F. η_{LoS} and η_{NLoS} are the additional attenuation factors for LoS and NLoS connections, respectively. Therefore, at the j-th slot, the channel gain between UAV k and the BS can be expressed as

$$g_{k,bs}^j\left(d_{k,bs}^j, f_k^j\right) = \frac{1}{PL_{k,bs}^j} = C_k^j (F + f_k^j)^{-2}, \tag{3}$$

where

$$C_k^j = \begin{cases} 10^{-32.4-\eta_{LoS}} \times (d_{k,bs}^j)^{-2}, & \text{LoS link} \\ 10^{-32.4-\eta_{NLoS}} \times (d_{k,bs}^j)^{-2}, & \text{NLoS link} \end{cases}$$

is the location dependent channel gain.

B. ADJACENT CHANNEL INTERFERENCE

To fully utilize the scarce spectrum resources, the available frequency bands for allocation are tightly segmented. The aggregate ACI cannot be neglected as multiple wireless devices are operating on adjacent channels simultaneously [17]. The existence of ACI effect is mainly ascribed to two reasons: on one hand, the terminal devices' receiver filters have limited performance; on the other hand, the side lobe effect of the BS' antenna may cause undesired

interference to terminal devices on the adjacent channels. Consider that the UAVs have the same type, and are equipped with the receiver filters that have similar properties. For any two UAVs u_1 and u_2, let f_1 and f_2 be the frequencies of their control channels, both the channels would suffer from the ACI. To quantify the effect of ACI leakage, we define a mapping function $\Psi : f_1, f_2 \mapsto \mu_{f_1,f_2}$ for f_1 and f_2, where μ_{f_1,f_2} is the ACI coefficient. Theoretically, μ_{f_1,f_2} satisfies the following properties:

$$\begin{cases} 0 \le \mu_{f_1,f_2} \le 1, \\ \mu_{f_1,f_2} = \mu_{f_2,f_1} \\ \mu_{f_1,f_2} = 1, \text{ if } |f_1 - f_2| = 0, \\ \mu_{f_1,f_2} \to 0, \text{ if } |f_1 - f_2| \to \infty, \\ 0 < \mu_{f_1,f_2} < 1, \text{ if } 0 < |f_1 - f_2| < \infty. \end{cases} \tag{4}$$

When $|f_1 - f_2| = 0$, which means u_1 and u_2 use the co-channel; $|f_1 - f_2| \to \infty$ represents that f_1 and f_2 are separated relatively far apart, hence the ACI is very weak. Notice that in practical system, μ_{f_1,f_2} can be determined by measurements.

C. PROBLEM FORMULATION

Without loss of generality, we consider a practical case that the time-frequency resources are limited, and only with the available channels or time slots alone are not sufficient for the communications between all the UAVs and the BS. To support the control signal reception of all the UAVs, the number of time-frequency RBs should not be less than the UAVs' number. Note that M, N and J represent the number of UAVs, available frequency bands and time slots, respectively, we have the following basic assumptions:

$$\begin{cases} M > \max\{N, J\}, \\ M \le N * J. \end{cases} \tag{5}$$

We define the matrix $\mathbf{S} \triangleq \left\{ s_k^j = \{0, 1\} \right\} \in \mathbb{R}^{M \times J}$ to indicate whether UAV k occupies a RB at slot j. If $s_k^j = 1$, which means UAV k takes a RB at the j-th slot; otherwise $s_k^j = 0$. Given the available time-frequency RBs, two actual constraints are considered: 1) Each UAV only occupies one RB; 2) Each RB can be assigned to at most one UAV. Mathematically, these constraints can be written as

$$\begin{cases} \sum_{j=1}^{J} s_k^j = 1, \quad \forall k \in \mathcal{M}, \\ f_k^j \ne f_m^j, k \ne m, \quad \forall j \in \mathcal{J}, \ \forall k, m \in \mathcal{M}. \end{cases} \tag{6}$$

On the UAVs side, the SINR level is used to measure the quality of the control signal. Based on the above definitions, at the j-th time slot, for UAV k, we formulate the SINR of the control signal at the receiver as followsl

$$\gamma_k^j = \frac{p_k C_k^j s_k^j \left(F + f_k^j\right)^{-2}}{\sum_{m \ne k} \mu_{f_k^j, f_m^j} p_m C_k^j s_m^j \left(F + f_m^j\right)^{-2} + \sigma_k^2}, \tag{7}$$

where $\boldsymbol{p} \triangleq \{p_k\} \in \mathbb{R}^{M \times 1}$ is the transmit power vector of the BS for each UAV, the aggregate ACI on the channel of UAV k at the same time slot is represented by $\sum_{m \ne k} \mu_{f_k^j, f_m^j} p_m C_k^j s_m^j \left(F + f_m^j\right)^{-2}$, and σ_k^2 is the power of additive white Gaussian noise (AWGN). When $s_k^j = 1$, the BS transmits signal to UAV k at slot j, hence $\gamma_k^j > 0$; whereas $\gamma_k^j = 0$ when $s_k^j = 0$. Since UAV k only occupies one time slot, the SINR of the control signal it received can be represented by

$$\gamma_k = \sum_{j=1}^{J} \gamma_k^j. \tag{8}$$

In general, the higher SINR of the control signal at a UAV, the more reliable information it might get from the BS. To improve the reliability of the control signal for all the UAVs, the corresponding SINR levels at UAVs should be promoted as far as possible. To this end, in this paper we adopt the max-min-fairness index among the SINR levels of UAVs, thus the objective value is determined by the UAV who has the lowest SINR level, and our goal is to maximize the lowest SINR by optimizing the time-frequency RBs assignment and the BS transmit power allocation. The problem of interest is formulated as

$$\max_{\left\{s_k^j, f_k^j, p_k\right\}} \min_k \left\{ \frac{p_k C_k^j s_k^j \left(F + f_k^j\right)^{-2}}{\sum_{m \ne k} \mu_{f_k^j, f_m^j} p_m C_k^j s_m^j \left(F + f_m^j\right)^{-2} + \sigma_k^2} \right\} \tag{9a}$$

$$\text{s.t.} \sum_{j=1}^{J} s_k^j = 1, \quad \forall k \in \mathcal{M}, \tag{9b}$$

$$f_k^j \ne f_m^j, k \ne m, \quad \forall j \in \mathcal{J}, \ \forall k, m \in \mathcal{M}, \tag{9c}$$

$$s_k^j \in \{0, 1\}, \quad \forall j \in \mathcal{J}, \ \forall k \in \mathcal{M}, \tag{9d}$$

$$f_k^j \in \{\textstyle\bigwedge f_1, \ldots, \bigwedge f_N\}, \quad \forall j \in \mathcal{J}, \ \forall k \in \mathcal{M}, \tag{9e}$$

$$\sum_{k=1}^{M} p_k \le P_{\max}, \tag{9f}$$

$$0 \le p_k, \quad \forall k \in \mathcal{M}, \tag{9g}$$

wherein (9f) means the maximum power constraint that the control BS can allocate to all the UAVs. Problem (9) is a Mixed-Integer Nonlinear Program (MINLP), which generally falls into the NP-hard category. Moreover, (9) is intractable for the typical optimization methods, because the optimization variables appears in the subscript (e.g., the variables $\{f_k^j\}$).

III. PROBLEM TRANSFORMATION

In this section, we firstly transform the difficult problem into a more tractable formulation, then we further leverage the rank-one property to further transform the problem into an equivalent but simpler form.

A. EQUIVALENT TRANSFORMATION VIA THE RB ASSIGNMENT MATRIX A

To make problem (9) tractable, we introduce the RB assignment matrix $\mathbf{A} \triangleq \left\{a_{i,j}^k | i \in \mathcal{N}, j \in \mathcal{J}, k \in \mathcal{M}\right\} \in \mathbb{R}^{N\times J\times M}$. For each UAV k, the matrix $\mathbf{A}_k = [\boldsymbol{a}_1^k, \ldots, \boldsymbol{a}_J^k]$ is defined to represent its RB occupancy pattern, where $\boldsymbol{a}_j^k = [a_{1,j}^k, \ldots, a_{N,j}^k]^T$. Specifically, $a_{i,j}^k = 1$ means the RB with respect to frequency band i and time slot j is assigned to UAV k, and $a_{i,j}^k = 0$ otherwise; when $\boldsymbol{a}_j^k = \mathbf{0}$, UAV k doesn't occupy the RB at slot j. Define $\boldsymbol{f} \triangleq \left[\triangle f_1, \ldots, \triangle f_N\right]^T$, and store the ACI coefficients in the symmetric matrix $\mathbf{W}$, namely $\mathbf{W}_{i,n} \triangleq \mu_{f_i,f_n}$, we have the following proposition.

Proposition 1: Problem (9) *can be equivalently transformed as* (10)*, as shown at the bottom of this page, where* $\boldsymbol{e}_j$ *is a unit column vector with the j-th element equals to 1.*

Proof: According to the definitions, we have the following equivalent transformations:

$$\begin{aligned} s_k^j &= \mathbf{1}^T \boldsymbol{a}_j^k = \mathbf{1}^T \mathbf{A}_k \boldsymbol{e}_j, \\ f_k^j &= \boldsymbol{f}^T \boldsymbol{a}_j^k = \boldsymbol{f}^T \mathbf{A}_k \boldsymbol{e}_j, \end{aligned} \tag{11}$$

and the ACI coefficient between the channels of UAV k and m at slot j is formulated as

$$\mu_{f_k^j, f_m^j} = (\boldsymbol{a}_j^k)^T \mathbf{W} \boldsymbol{a}_j^m = (\mathbf{A}_k \boldsymbol{e}_j)^T \mathbf{W} \mathbf{A}_m \boldsymbol{e}_j. \tag{12}$$

As a direct result, problem (9) is transformed into (10), wherein the constraints (10b) and (10c) correspond to (9b) and (9c), respectively; constraint (10d) corresponds to (9d) and (9e), and other constraints remain unchanged. ■

Note that although problem (10) is still a MINLP, its form is more concise and tractable than (9), and we can directly deal with problem (10), later we will show that problem (10) could be further transformed into another equivalent form, which is very suitable for efficient algorithms design.

B. EQUIVALENT TRANSFORMATION VIA THE CHANNEL OCCUPANCY MATRIX X AND THE SLOT OCCUPANCY MATRIX Y

From (10), it is observed that $\mathbf{A}_k, k = \{1, \ldots, M\}$ are coupling in constraint (10c), which makes it difficult to design efficient algorithms. Another drawback of (10) is that matrix $\mathbf{A}$ contains NJM elements, with so many optimization variables it would be challenging to find low complexity algorithms.

We notice that matrix $\mathbf{A}_k, \forall k \in \mathcal{M}$ contains only one nonzero element, hence each $\mathbf{A}_k$ satisfies the rank-one property, which implies that each $\mathbf{A}_k$ can be substituted by low dimensional vectors. Based on this idea, we can represent problem (10) in a simpler form. We try to reach this target by introducing two key matrices: the channel occupancy matrix $\mathbf{X} \triangleq \left[\boldsymbol{x}^1, \ldots, \boldsymbol{x}^M\right] \in \mathbb{R}^{N\times M}$ and the slot occupancy matrix $\mathbf{Y} \triangleq \left[\boldsymbol{y}^1, \ldots, \boldsymbol{y}^M\right] \in \mathbb{R}^{J\times M}$, where $\boldsymbol{x}^k = \left[x_1^k, \ldots, x_n^k\right]^T$ and $\boldsymbol{y}^k = \left[y_1^k, \ldots, y_n^k\right]^T$. For $\mathbf{X}$, the element $x_i^k = 1$ indicates that UAV k occupies the channel i, otherwise $x_i^k = 0$; for $\mathbf{Y}$, $y_j^k = 1$ indicates that UAV k occupies the slot j, otherwise $y_j^k = 0$.

Moreover, we hope that the constraint (10c) can be decoupled, meanwhile different UAVs are forced to occupy different RBs. We consider to achieve this effect via adapting the ACI coefficient matrix $\mathbf{W}$, then we can obtain the following proposition.

Proposition 2: Define the matrices $\mathbf{X}$ *and* $\mathbf{Y}$*, and let the diagonal elements of* $\mathbf{W}$ *be sufficiently large, then problem* (10) *can be simplified as* (13)*, as shown at the bottom of this page.*

$$\max_{\{\mathbf{A}_k, p_k\}} \min_k \sum_{j=1}^{J} \frac{p_k C_k^j \mathbf{1}^T \mathbf{A}_k \boldsymbol{e}_j \left(F + \boldsymbol{f}^T \mathbf{A}_k \boldsymbol{e}_j\right)^{-2}}{\sum\limits_{m\neq k}^{M} \left(\mathbf{A}_m \boldsymbol{e}_j\right)^T \mathbf{W} \mathbf{A}_k \boldsymbol{e}_j p_m C_k^j \mathbf{1}^T \mathbf{A}_m \boldsymbol{e}_j \left(F + \boldsymbol{f}^T \mathbf{A}_m \boldsymbol{e}_j\right)^{-2} + \sigma_k^2} \tag{10a}$$

$$\text{s.t. } \mathbf{1}^T \mathbf{A}_k \mathbf{1} = 1, \quad \forall k \in \mathcal{M}, \tag{10b}$$

$$\sum_{k=1}^{M} \mathbf{A}_k \leq \mathbf{E}_{N\times J}, \tag{10c}$$

$$a_{i,j}^k \in \{0, 1\}, \quad \forall i \in \mathcal{N}, \ \forall j \in \mathcal{J}, \forall k \in \mathcal{M}, \tag{10d}$$

$$\text{(9f), (9g).} \tag{10e}$$

$$\max_{\{\boldsymbol{x}^k, \boldsymbol{y}^k, p_k\}} \min_k \sum_{j=1}^{J} \frac{p_k C_k^j \boldsymbol{e}_j^T \boldsymbol{y}^k \left(F + \boldsymbol{f}^T \boldsymbol{x}^k \boldsymbol{e}_j^T \boldsymbol{y}^k\right)^{-2}}{\sum\limits_{m\neq k}^{M} p_m C_k^j \boldsymbol{e}_j^T \boldsymbol{y}^m (\boldsymbol{x}^m)^T \mathbf{W} \boldsymbol{x}^k \boldsymbol{e}_j^T \boldsymbol{y}^k \left(F + \boldsymbol{f}^T \boldsymbol{x}^m \boldsymbol{e}_j^T \boldsymbol{y}^m\right)^{-2} + \sigma_k^2} \tag{13a}$$

$$\text{s.t. } \mathbf{1}^T \boldsymbol{x}^k = 1, \quad \forall k \in \mathcal{M}, \tag{13b}$$

$$\mathbf{1}^T \boldsymbol{y}^k = 1, \quad \forall k \in \mathcal{M}, \tag{13c}$$

$$x_i^k \in \{0, 1\}, \quad \forall i \in \mathcal{N}, \ \forall k \in \mathcal{M}, \tag{13d}$$

$$y_j^k \in \{0, 1\}, \quad \forall j \in \mathcal{J}, \ \forall k \in \mathcal{M}, \tag{13e}$$

$$\text{(9f), (9g).} \tag{13f}$$

Proof: Based on the definitions of $\mathbf{X}$ and $\mathbf{Y}$, we have $\mathbf{1}^T\boldsymbol{x}^k = \mathbf{1}^T\boldsymbol{y}^k = 1$, and $\mathbf{A}_k \triangleq \boldsymbol{x}^k \left(\boldsymbol{y}^k\right)^T$ for $\forall k \in \mathcal{M}$, as well as the following equivalent transformations:

$$\begin{aligned} \mathbf{1}^T\mathbf{A}_k\boldsymbol{e}_j &= \boldsymbol{e}_j^T\boldsymbol{y}^k, \\ \mathbf{A}_k\boldsymbol{e}_j &= \boldsymbol{x}^k\boldsymbol{e}_j^T\boldsymbol{y}^k, \\ \boldsymbol{f}^T\mathbf{A}_k\boldsymbol{e}_j &= \boldsymbol{f}^T\boldsymbol{x}^k\boldsymbol{e}_j^T\boldsymbol{y}^k. \end{aligned} \tag{14}$$

Because $\boldsymbol{e}_j^T\boldsymbol{y}^m = \{0, 1\} = \left(\boldsymbol{e}_j^T\boldsymbol{y}^m\right)^2$, we can represent the aggregate ACI by

$$\sum_{m\neq k}^{M} p_m C_k^j \boldsymbol{e}_j^T\boldsymbol{y}^m \left(\boldsymbol{x}^m\right)^T \mathbf{W}\boldsymbol{x}^k\boldsymbol{e}_j^T\boldsymbol{y}^k \left(F + \boldsymbol{f}^T\boldsymbol{x}^m\boldsymbol{e}_j^T\boldsymbol{y}^m\right)^{-2}, \tag{15}$$

If the diagonal elements of $\mathbf{W}$ are getting large, then the term $(\boldsymbol{a}_j^k)^T\mathbf{W}\boldsymbol{a}_j^m$ increases for $\boldsymbol{a}_j^k = \boldsymbol{a}_j^m$, thus the co-channel interference would be stronger, consequently UAVs tend to occupy different RBs for higher SINR levels, therefore the constraints (10c) can be decoupled.

As a result, problem (10) can be simplified as (13), where constraints (13b) and (13c) correspond to (10b), the coupling constraint (10c) is replaced by setting sufficiently large value for $\mathbf{W}$'s diagonal elements in (13a), the constraints (13d) and (13e) correspond to (10d), and the constraints with respect to $\boldsymbol{p}$ are unchanged. ■

Proposition 1 and 2 suggest that the optimal solution to problem (9) can be obtained by solving problem (13), hence the main task of the rest paper is to solve problem (13). In (13), we observe that the constraints are separable across the variables $\mathbf{X}$ and $\mathbf{Y}$. Moreover, the total number of elements in $\mathbf{X}$ and $\mathbf{Y}$ is $M(N + J)$, which is much less than that of $\mathbf{A}$. In the sequel, to solve (13), we first propose a low complexity method based on the BCD method in Section IV; then, to approximate the best system performance, we further propose an optimization method based on smooth approximation and gradient projection in Section V.

IV. BLOCK COORDINATE DESCENT BASED METHOD

Since the constraints of (13) are separable across the variables $\mathbf{X}$, $\mathbf{Y}$ and $\boldsymbol{p}$, we can use the BCD method to optimize the RBs assignment and BS transmit power iteratively. The proposed BCD-based method alternately updates the $\mathbf{X}$, $\mathbf{Y}$ block and $\boldsymbol{p}$ block, one at a time with the other being fixed. In the following, we first propose a BCD-based method to update $\mathbf{X}$ and $\mathbf{Y}$,[1] then use the eigenvalue decomposition method to update $\boldsymbol{p}$.

A. UPDATE X and Y VIA THE BCD-BASED METHOD

The optimization of $\mathbf{X}$ and $\mathbf{Y}$ with $\boldsymbol{p}$ fixed is a combinational problem, because the constraints are separable over $\mathbf{X}$ and $\mathbf{Y}$,

[1]Need to mention that the proposed BCD-based method for updating $\mathbf{X}$ and $\mathbf{Y}$ does not regard the matrices $\mathbf{X}$ and $\mathbf{Y}$ as two independent blocks. Each time, given any UAV index, i.e. m, it is that the corresponding vectors $\boldsymbol{x}^m$ and $\boldsymbol{y}^m$ in $\mathbf{X}$ and $\mathbf{Y}$ are optimized in the BCD manner.

Algorithm 1 Block Coordinate Descent Based Method for Updating $\mathbf{X}$ and $\mathbf{Y}$

1: **Initialize** $\mathbf{X}^{(0)}$ and $\mathbf{Y}^{(0)}$, and define the maximum iteration number $T_{1,\max}$, set $t = 0$.
2: **repeat**
3: Set $\mathbf{X} = \mathbf{X}^{(t)}$, $\mathbf{Y} = \mathbf{Y}^{(t)}$, generate a random permutation $\Theta^{(t)}$ containing the integers from 1 to M, set $k = 0$.
4: **repeat**
5: Set $k = k + 1$, and $m = \Theta^{(t)}(k)$.
6: Fix $\mathbf{Y}$ and $\mathbf{X}_{-m}$, update $\boldsymbol{x}^m = \boldsymbol{e}_I$, where

$$I = \underset{i\in\{1,\ldots,N\}}{\operatorname{argmax}} f\left(\left(\mathbf{X}_{-m}, \boldsymbol{e}_i\right), \mathbf{Y}, \boldsymbol{p}\right). \tag{16}$$

7: Fix $\mathbf{X}$ and $\mathbf{Y}_{-m}$, update $\boldsymbol{y}^m = \boldsymbol{e}_K$, where

$$K = \underset{j\in\{1,\ldots,J\}}{\operatorname{argmax}} f\left(\mathbf{X}, \left(\mathbf{Y}_{-m}, \boldsymbol{e}_j\right), \boldsymbol{p}\right). \tag{17}$$

8: **until** $k = M$.
9: Set $t = t + 1$, and $\mathbf{X}^{(t)} = \mathbf{X}$, $\mathbf{Y}^{(t)} = \mathbf{Y}$.
10: **until** the objective value is unchanged, or maximum iteration number is reached.

we can also alternatively optimize $\mathbf{X}$ and $\mathbf{Y}$. Our main idea is to locally optimize each UAV via coordinate descent. For a UAV k, we can find the best $\boldsymbol{x}^k$ and $\boldsymbol{y}^k$ while keeping $\{\boldsymbol{x}^m, \boldsymbol{y}^m\}$, $\forall m \neq k$ fixed, and then repeat the same step to optimize other UAVs. Accordingly, the proposed BCD-based method for updating $\mathbf{X}$ and $\mathbf{Y}$ is summarized in Algorithm 1. Specifically, the initial values of $\mathbf{X}$ and $\mathbf{Y}$ in Algorithm 1 are provided by the outer algorithm. Each time we select a UAV from the random permutation vector $\Theta^{(t)}$ in turn, whose elements represent the index of all the UAVs. Define $\mathbf{X} \triangleq (\mathbf{X}_{-k}, \boldsymbol{x}^k)$, and $\mathbf{Y} \triangleq (\mathbf{Y}_{-k}, \boldsymbol{y}^k)$, where $\mathbf{X}_{-k}$ and $\mathbf{Y}_{-k}$ are the columns of matrices $\mathbf{X}$ and $\mathbf{Y}$ except the k-th column, respectively. Denote $f(\mathbf{X}, \mathbf{Y}, \boldsymbol{p})$ as the objective value of (13), for the selected UAV index m, we first find the best $\boldsymbol{x}_m$ by fixing $\mathbf{Y}$ and $\mathbf{X}_{-m}$ in Step 6, then the best $\boldsymbol{y}_m$ is found in Step 7. Through these steps, the objective value of (13) keeps increasing iteratively. For the complexity of this method, according to (16) and (17), each chosen UAV needs to evaluate the objective value at most $N + J$ times one iteration. Given the required iterations number T_1, Algorithm 1 needs at most $T_1\, M(N + J)$ evaluations.

B. UPDATE p VIA THE EIGENVALUE DECOMPOSITION METHOD

Given the values of $\mathbf{X}$ and $\mathbf{Y}$, we can rewrite (13) as the following power optimization problem

$$\max_{\{p_k\}} \min_k \left\{ \frac{p_k b_{k,k}}{\sum_{m\neq k}^{M} p_m b_{k,m} + \sigma_k^2} \right\} \tag{18a}$$

$$\text{s.t.} \sum_{k=1}^{M} p_k \le P_{\max}, \tag{18b}$$

$$0 \le p_k, \quad \forall k \in \mathcal{M}, \tag{18c}$$

where $b_{k,m}, \forall k, m \in \mathcal{M}$ are constant coefficients, which are determined by $\mathbf{X}$ and $\mathbf{Y}$. Although (18) is non-convex, we can solve problems of this form efficiently based on the conclusion in [18]. Define $\boldsymbol{z} = [p_1, \ldots, p_M, 1]^T$, $\gamma = \frac{p_k b_{k,k}}{\sum_{m \ne k}^{M} p_m b_{k,m} + \sigma_k^2}, \forall k$, and

$$\mathbf{C} = \begin{bmatrix} \mathbf{I}_{M\times M} & \mathbf{0}_{M\times 1} \\ \mathbf{1}_{1\times M} & -P_{\max} \end{bmatrix}, \quad \mathbf{B} = \begin{bmatrix} \mathbf{R}_{M\times M} & \boldsymbol{h} \\ \mathbf{0}_{1\times M} & 0 \end{bmatrix},$$

where

$$\mathbf{R} = \begin{cases} \frac{b_{k,m}}{b_{k,k}}, & k \ne m \\ 0, & k = m \end{cases}, \quad \boldsymbol{h} = \left[\frac{\sigma_1^2}{b_{1,1}}, \ldots, \frac{\sigma_M^2}{b_{M,M}} \right]^T.$$

Whenever constraint (18b) holds with strict inequality, we can scale $\{p_k\}$ proportionally to improve the objective value of (18), so (18b) could be written as an equality constraint. Based on the above definitions, we can represent the constraint of (18) as

$$\mathbf{C}\boldsymbol{z} = \gamma \mathbf{B}\boldsymbol{z}, \tag{19}$$

equivalently, we have $\frac{1}{\gamma}\boldsymbol{z} = \mathbf{C}^{-1}\mathbf{B}\boldsymbol{z}$, therefore $\frac{1}{\gamma}$ is the eigenvalue of the non-negative matrix $\mathbf{C}^{-1}\mathbf{B}$, and $\boldsymbol{z}$ is the corresponding eigenvector. According to [18] and the property of non-negative matrix, for $\mathbf{C}^{-1}\mathbf{B}$, the eigenvalue of the largest norm is positive, and its corresponding eigenvector can be chosen to be non-negative. The optimal value of (18) is the reciprocal of the largest eigenvalue of $\mathbf{C}^{-1}\mathbf{B}$, which is given by

$$\gamma = 1/\lambda_{\max}(\mathbf{C}^{-1}\mathbf{B}), \tag{20}$$

and this result implies that all the UAVs would obtain the equal SINR levels. Let $\boldsymbol{z}$ be the eigenvector with respect to the largest eigenvalue, we can scale this vector such that the last element is 1, then the first M elements offer the optimal solution of (18).

To sum up, we present the proposed BCD-based method for solving (13) in Algorithm 2. The initial value of $\boldsymbol{p}$ can be simply set as $p_k = \frac{P_{\max}}{M}, \forall k$, while the values of $\mathbf{X}$ and $\mathbf{Y}$ could be initialized in a random manner considering their constraints. When $T_{1,\max} = 1$, Algorithm 2 only optimize $\mathbf{X}$, $\mathbf{Y}$ and $\boldsymbol{p}$ once each time; whereas when $T_{1,\max}$ is large, which means $\mathbf{X}$ and $\mathbf{Y}$ are optimized thoroughly before optimizing $\boldsymbol{p}$.

V. SMOOTH APPROXIMATION AND GRADIENT PROJECTION BASED METHOD

In general, the BCD optimization algorithm is effectively applied to continuous problems. For the discrete cases, the BCD method might be trapped into the local points. In addition, the global optimum of such kind of problem is

Algorithm 2 Block Coordinate Descent Based Method for Solving problem (13)

1: **Initialize** $\boldsymbol{p}$, $\mathbf{X}$, $\mathbf{Y}$, and define the maximum iteration number $T_{2,\max}$.
2: **repeat**
3: Fix $\boldsymbol{p}$, use Algorithm 1 to update $\mathbf{X}$ and $\mathbf{Y}$.
4: Fix $\mathbf{X}$ and $\mathbf{Y}$, update $\boldsymbol{p}$ by using (19) to solve problem (18).
5: **until** the objective value converges, or the maximum iteration number is reached.

hardly to achieve, for this reason, we hope to approximate the best performance of problem (13) by continuous optimization methods. Therefore, we consider to relax the binary variables $\mathbf{X}$ and $\mathbf{Y}$ into continuous variables, then solve this relaxed continuous problem. Ultimately, $\mathbf{X}$ and $\mathbf{Y}$ can be determined by rounding the optimization results. If the elements of the optimized $\mathbf{X}$ and $\mathbf{Y}$ don't have evident tendency toward 0 or 1, we can strengthen this effect by adding proper penalty term to the objective function. Nevertheless, for problem (13), after relaxing $\mathbf{X}$ and $\mathbf{Y}$ into the variables within [0, 1], we observe a peculiar phenomenon: *when the value of numerator in the objective function is very small, we have* $\boldsymbol{e}_j^T\boldsymbol{y}^k \ll 1$, *which indicates that UAV k won't occupy the RBs at the j-th slot, and the corresponding SINR should be low. However, due to the joint effects of* $\boldsymbol{e}_j^T\boldsymbol{y}^m$ *and* $\boldsymbol{e}_j^T\boldsymbol{y}^k$, *the denominator is much less than the numerator in the objective function, consequently the SINR level for UAV k at slot j is very large instead.* This phenomenon doesn't get improved even if the penalty term is added. Hence, we couldn't obtain the desirable RBs assignment by directly optimizing the relaxed formulation of (13).

The above analyses explain that the relaxation of the term $\boldsymbol{e}_j^T\boldsymbol{y}^k$ for (13) will be counterproductive. The reason behind is that in the expression of SINR, when the value of $\{\boldsymbol{e}_j^T\boldsymbol{y}^k\}$ decreases, the denominator will experience faster attenuation than the numerator. We hope to avoid this phenomenon after relaxation, while not changing the physical meaning of the objective function of (13). We know that the value of $\boldsymbol{e}_j^T\boldsymbol{y}^k$ is either 0 or 1 before relaxation, hence

$$\left(\boldsymbol{e}_j^T\boldsymbol{y}^k\right)^n = \boldsymbol{e}_j^T\boldsymbol{y}^k, n \ge 1. \tag{21}$$

If n is sufficiently large, in the objective function of (13), after relaxation the numerator will be attenuating much faster than the denominator as $\boldsymbol{e}_j^T\boldsymbol{y}^k$ decreases, thus we can overcome the challenge that the numerator is very small, but the corresponding SINR is large. To see the effect of the exponential coefficient n, the authors may refer to the detailed simulation results in Section VI-B. According to the analyses, we can equivalently write (13) as (22), as shown at the bottom of the next page.

In the following, for (22), we approximate this noncontinuous problem as a smooth one, and then propose a gradient projection (GP) based method to solve it.

A. SMOOTH APPROXIMATION

We first give a smooth approximation for the objective of the problem (23), by using the following lemma.

Lemma 1: According to [19], the following inequality holds

$$\max\{x_1,\ldots,x_n\} \le f(x) \le \max\{x_1,\ldots,x_n\} + \mu \log n, \tag{23}$$

where

$$f(x) = \mu \log\left(\exp\left(\frac{x_1}{\mu}\right) + \cdots + \exp\left(\frac{x_n}{\mu}\right)\right), \quad \mu > 0, \tag{24}$$

when μ is sufficiently small, we can approximate

$$f(x) \approx \max\{x_1,\ldots,x_n\}. \tag{25}$$

According to Lemma 1, we define $f_k(\mathbf{X},\mathbf{Y},\boldsymbol{p})$ as the expression in (26), as shown at the bottom of this page.

Then we have

$$\begin{aligned} f_\mu(\mathbf{X},\mathbf{Y},\boldsymbol{p}) &= \mu \log \sum_{k=1}^{M} \exp\left(\frac{f_k(\mathbf{X},\mathbf{Y},\boldsymbol{p})}{\mu}\right) \\ &\approx \max\left\{f_1(\mathbf{X},\mathbf{Y},\boldsymbol{p}),\ldots,f_M(\mathbf{X},\mathbf{Y},\boldsymbol{p})\right\}, \end{aligned} \tag{27}$$

with a small μ. Hence problem (13) can be approximated as the following problem

$$\begin{aligned} -\min_{\{\boldsymbol{x}^k,\boldsymbol{y}^k,p_k\}} \; & f_\mu(\mathbf{X},\mathbf{Y},\boldsymbol{p}) \\ \text{s.t. } & \text{(9f), (9g), (13b)-(13e).} \end{aligned} \tag{28}$$

We further relax the binary integer variables $\mathbf{X}$ and $\mathbf{Y}$, then problem (28) is transformed into a continuous problem

$$\min_{\{\boldsymbol{x}^k,\boldsymbol{y}^k,p_k\}} \; f_\mu(\mathbf{X},\mathbf{Y},\boldsymbol{p}) \tag{29a}$$

$$\text{s.t. } \mathbf{1}^T\boldsymbol{x}^k = 1, \forall k \in \mathcal{M}, \tag{29b}$$

$$\mathbf{1}^T\boldsymbol{y}^k = 1, \quad \forall k \in \mathcal{M}, \tag{29c}$$

$$0 \le x_i^k, \quad \forall i \in \mathcal{N},\ \forall k \in \mathcal{M}, \tag{29d}$$

$$0 \le y_j^k, \quad \forall j \in \mathcal{J},\ \forall k \in \mathcal{M}, \tag{29e}$$

$$\text{(9f), (9g).} \tag{29f}$$

Algorithm 3 Gradient Projection Based Method for Solving Problem (22)

1: **Initialize** $\boldsymbol{p}$, $\mathbf{X}$, $\mathbf{Y}$. Define the tolerance of accuracy ϵ_3 and the maximum iteration number $T_{3,\max}$.
2: **repeat**
3: Calculate the gradients: $\nabla_{\mathbf{X}} f_\mu(\mathbf{X},\mathbf{Y},\boldsymbol{p})$, $\nabla_{\mathbf{Y}} f_\mu(\mathbf{X},\mathbf{Y},\boldsymbol{p})$ and $\nabla_{\boldsymbol{p}} f_\mu(\mathbf{X},\mathbf{Y},\boldsymbol{p})$.
4: Calculate the projections:

$$\mathbf{X}_{proj} = P_{\Omega_{\mathbf{X}}}\left(\mathbf{X} - \nabla_{\mathbf{X}} f_\mu(\mathbf{X},\mathbf{Y},\boldsymbol{p})\right),$$

$$\mathbf{Y}_{proj} = P_{\Omega_{\mathbf{Y}}}\left(\mathbf{Y} - \nabla_{\mathbf{Y}} f_\mu(\mathbf{X},\mathbf{Y},\boldsymbol{p})\right),$$

$$\boldsymbol{p}_{proj} = P_{\Omega_{\boldsymbol{p}}}\left(\boldsymbol{p} - \nabla_{\boldsymbol{p}} f_\mu(\mathbf{X},\mathbf{Y},\boldsymbol{p})\right).$$

5: Update $\mathbf{X}$, $\mathbf{Y}$ and $\boldsymbol{p}$ according to (30)

$$\begin{pmatrix}\mathbf{X}\\ \mathbf{Y}\\ \boldsymbol{p}\end{pmatrix} \longleftarrow \begin{pmatrix}\mathbf{X}\\ \mathbf{Y}\\ \boldsymbol{p}\end{pmatrix} + \alpha \begin{pmatrix}\mathbf{X}_{proj}-\mathbf{X}\\ \mathbf{Y}_{proj}-\mathbf{Y}\\ \boldsymbol{p}_{proj}-\boldsymbol{p}\end{pmatrix}. \tag{30}$$

6: **until** the objective value of $f_\mu(\mathbf{X},\mathbf{Y},\boldsymbol{p})$ converges, or the maximum iteration number is reached.
7: Round the elements of $\mathbf{X}$ and $\mathbf{Y}$ into 0-1 integers.
8: Put $\mathbf{X}$ and $\mathbf{Y}$ into (22), and optimize $\boldsymbol{p}$ by the eigenvalue decomposition method.

B. PROPOSED GRADIENT PROJECTION BASED METHOD

Note that the objective function of problem (29) is continuous and differentiable with respect to $\mathbf{X}$, $\mathbf{Y}$ and $\boldsymbol{p}$, we also observe that the constraints of $\mathbf{X}$, $\mathbf{Y}$, $\boldsymbol{p}$ are independent probability simplex. Since the projection of any point onto the probability simplex is simple to compute by sophisticated methods [20], [21], we can easily apply the gradient projection method to solve problem (29). After obtaining the solution of (29), we can determine the ultimate value of $\mathbf{X}$, $\mathbf{Y}$, $\boldsymbol{p}$ accordingly, the detailed steps for solving (22) based on GP method is summarized in Algorithm 3.

$$\max_{\{\boldsymbol{x}^k,\boldsymbol{y}^k,p_k\}} \; \min_k \sum_{j=1}^{J} \frac{p_k C_k^j \left(\boldsymbol{e}_j^T\boldsymbol{y}^k\right)^n \left(F + \boldsymbol{f}^T\boldsymbol{x}^k\boldsymbol{e}_j^T\boldsymbol{y}^k\right)^{-2}}{\sum\limits_{m\ne k}^{M} p_m C_k^j \boldsymbol{e}_j^T\boldsymbol{y}^m (\boldsymbol{x}^m)^T \mathbf{W}\boldsymbol{x}^k\boldsymbol{e}_j^T\boldsymbol{y}^k \left(F + \boldsymbol{f}^T\boldsymbol{x}^m\boldsymbol{e}_j^T\boldsymbol{y}^m\right)^{-2} + \sigma_k^2}$$

$$\text{s.t. (9f), (9g), (13b)-(13e).} \tag{22}$$

$$f_k(\mathbf{X},\mathbf{Y},\boldsymbol{p}) \triangleq -\sum_{j=1}^{J} \frac{p_k C_k^j \left(\boldsymbol{e}_j^T\boldsymbol{y}^k\right)^n \left(F + \boldsymbol{f}^T\boldsymbol{x}^k\boldsymbol{e}_j^T\boldsymbol{y}^k\right)^{-2}}{\sum\limits_{m\ne k}^{M} p_m C_k^j \boldsymbol{e}_j^T\boldsymbol{y}^m (\boldsymbol{x}^m)^T \mathbf{W}\boldsymbol{x}^k\boldsymbol{e}_j^T\boldsymbol{y}^k \left(F + \boldsymbol{f}^T\boldsymbol{x}^m\boldsymbol{e}_j^T\boldsymbol{y}^m\right)^{-2} + \sigma_k^2} \tag{26}$$

Let $\mathbf{X} \in \Omega_{\mathbf{X}}$, $\mathbf{Y} \in \Omega_{\mathbf{Y}}$ and $\boldsymbol{p} \in \Omega_{\boldsymbol{p}}$, where $\Omega_{\mathbf{X}} \triangleq \left\{\mathbf{1}^T\boldsymbol{x}^k = 1, x_i^k \in [0,1], \forall i,k\right\}$, $\Omega_{\mathbf{Y}} \triangleq \left\{\mathbf{1}^T\boldsymbol{y}^k = 1, y_j^k \in [0,1], \forall j,k\right\}$ and $\Omega_{\boldsymbol{p}} \triangleq \left\{\sum_{k=1}^{M} p_k = P_{\max}, 0 \le p_k, \forall k\right\}$. In the first step of Algorithm 3, we randomly initialize the elements of $\mathbf{X}$ and $\mathbf{Y}$, and $\boldsymbol{p}$. For any given matrix $\bar{\mathbf{X}} \in \mathbb{R}^{N\times M}$, the projection of $\bar{\mathbf{X}}$ onto the simplex $\Omega_{\mathbf{X}}$ is to solve the minimization problem

$$\mathbf{X} = \underset{\mathbf{X}\in\Omega_{\mathbf{X}}}{\operatorname{argmin}} \|\mathbf{X} - \bar{\mathbf{X}}\|, \tag{31}$$

we denote this projection problem as $P_{\Omega_{\mathbf{X}}}(\bar{\mathbf{X}})$, the notations of $P_{\Omega_{\mathbf{Y}}}(\cdot)$ and $P_{\Omega_{\boldsymbol{p}}}(\cdot)$ are expressed similarly. In step 3, the gradients point out a descending direction for the objective function, whereas Step 4 projects a point onto the feasible set of (29). In Step 5, $\alpha \ge 0$ is a judiciously chosen step size, which can be determined based on the Armijo's rule [22]. The objective value of $f_\mu(\mathbf{X},\mathbf{Y},\boldsymbol{p})$ is monotonically decreasing through the iterations from Step 3 to Step 5, but problem (29) doesn't need to be thoroughly optimized, the iterations can be terminated as long as the elements in $\mathbf{X}$ and $\mathbf{Y}$ are already shown evident tendency toward 0 or 1. Once the iterations of gradient projection are finished, the ultimate values of $\mathbf{X}$ and $\mathbf{Y}$ can be determined by simply rounding their elements into 0-1 integers, then the problem (22) with respect to $\boldsymbol{p}$ is reduced to problem (18), which could be solved by the eigenvalue decomposition method. To speed up the convergence for the gradient projection iterations from Step 3 to Step 6, we can also introduce a penalty term in the objective function (29a). Following [23], we use the binary nature of $\mathbf{X}$ or $\mathbf{Y}$ to enforce $x_i^k = (x_i^k)^2$ or $y_j^k = (y_j^k)^2$, then (29a) can be substituted by the new objective function, which is defined as

$$L_{\mu,\lambda}(\mathbf{X},\mathbf{Y},\boldsymbol{p}) \triangleq f_\mu(\mathbf{X},\mathbf{Y},\boldsymbol{p}) + \lambda \sum_{k=1}^{M}\sum_{i=1}^{N}\left[x_i^k - (x_i^k)^2\right], \tag{32}$$

where $\lambda \ge 0$ is a constant penalty factor, which signifies the relative importance of recovering binary values for $\mathbf{X}$ over the minimization of $f_\mu(\mathbf{X},\mathbf{Y},\boldsymbol{p})$.

VI. SIMULATION RESULTS

In this section, simulation results are presented to validate the performance of the proposed algorithms. We consider a system that the UAVs are flying in a 3D space, and the projection plane onto ground is a 2D area of $5 \times 5\,\text{km}^2$, where the control BS is located in the center. The UAV's flying altitude is permitted to range from 100 m to 2.5 km, while the minimum height corresponds to the minimum altitude required in moderate mountains area. Considering the high speed fixed-wing or hybrid fixed-and-rotary-wing UAVs, the maximum UAV velocity is $V_{\max} = 50$ m/s [13]. To determine the UAV' trajectory coordinates in a specified time period, the central processing unit at the control BS could plan in advance or calculate by the UAV' current state information. Given the UAVs' initial coordinates, their flying velocity vectors and the time interval between different time slots, then the trajectory coordinates of UAVs over each slots are deduced. The channel gains between UAVs and the BS are generated based on the model from (1) to (3) while considering the LoS and NLoS occurrence probabilities. For simplicity, we assume the interval between each channel is the same, and the noise powers at the UAVs' receivers are identical and given by $\sigma_1^2 = \ldots = \sigma_M^2 \triangleq \sigma^2$. For the ACI coefficients, we refer to the measurement results of [24] for the modeling of matrix $\mathbf{W}$. The related simulation parameters are listed in Table 1, part of them are set based on the typical values as those in [4] and [14].

TABLE 1. Simulation parameters.

Description	Parameter	Value
Baseline carrier frequency	F	500 MHz
Channel interval	$\triangle f_1 = \ldots = \triangle f_N$	5 MHz
Maximum transmit power of the control BS	$P_{\max}$	30 dBm
Additional path loss for LoS	η_{LoS}	3 dB
Additional path loss for NLoS	η_{NLoS}	23 dB
Parameter for dense urban environment	B, C	0.136, 11.95
Noise power	σ^2	-90 dBm

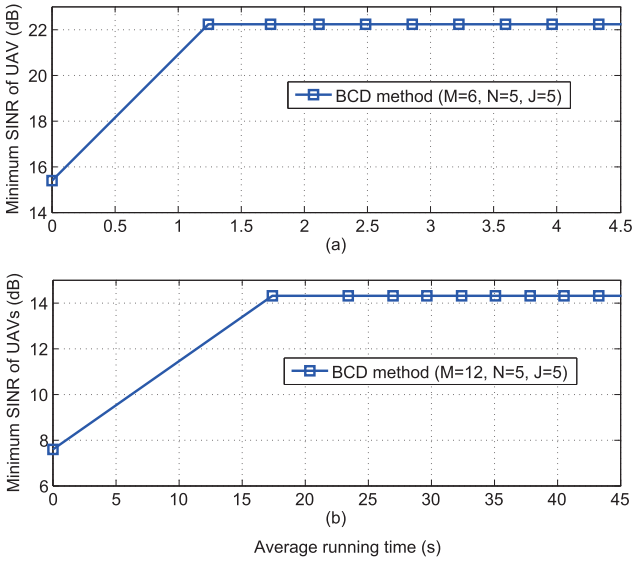

FIGURE 2. The minimum SINR levels of UAVs versus the average running time.

A. CONVERGENCE EVALUATION

In this subsection, we examine the convergence of the proposed algorithms by setting the number of available channels and time slots as $N = 5$ and $J = 5$. Both these two algorithms are implemented with the Core i7, 2.6 GHz CPUs. Fig. 2 and Fig. 3 show the convergence behaviors of the proposed BCD-based method and GP-based method, respectively. For the BCD-based method, to avoid the algorithm converging to the undesired local points prematurely, we set the

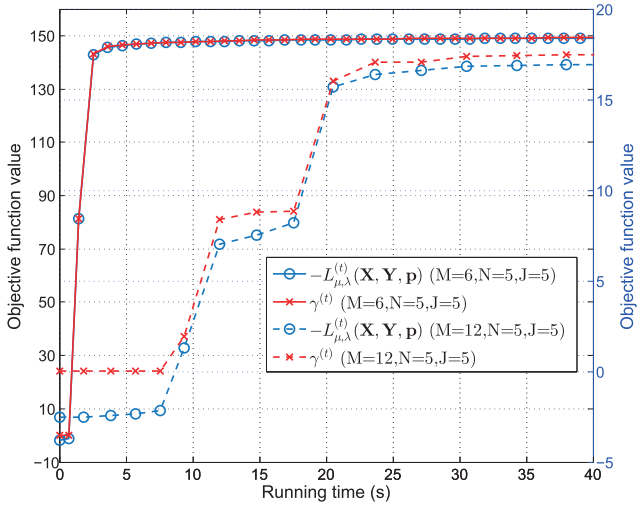

FIGURE 3. The objective function value versus the algorithm running time.

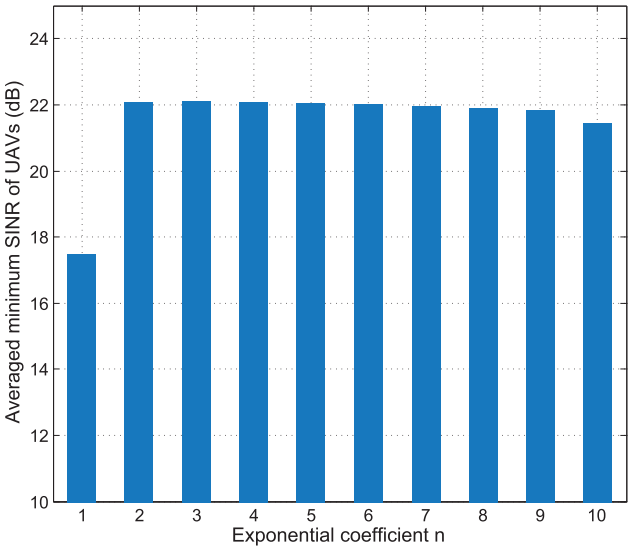

FIGURE 4. Impact of the exponential coefficient n on the system performance ($M = 6, N = 5, J = 5$).

maximum iteration number in Algorithm 1 as $T_{1,\max} = 10$, which is sufficient for the convergence of Algorithm 1. Fig. 2 presents the averaged results of multiple independent running of Algorithm 2 for solving (13). Since the computation complexity of $\boldsymbol{p}$ with the eigenvalue decomposition method is trivial, the total computation complexity of Algorithm 2 equals to the complexity of Algorithm 1. When the number of UAVs is $M = 6$, Algorithm 1 converges very fast, therefore Algorithm 2 can converge in 1.3 seconds; when $M = 12$, Algorithm 2 needs 17.4 seconds to converge, which is due to that in Algorithm 1, more UAVs are needed to evaluate, and the convergence needs more iterations.

Fig. 3 plots the objective function value against the running times of the gradient projection iterations from the Step 3 to Step 6 in Algorithm 3. The objective function $L_{\mu,\lambda}(\mathbf{X},\mathbf{Y},\boldsymbol{p})$ is optimized with Algorithm 3 for solving (29) under the setting of $\mu = 1$ and $\lambda = \frac{1}{5MN}$, and γ represents the objective function value of (22). Based on the smooth approximation theory in Section V-A and the definition of $L_{\mu,\lambda}(\mathbf{X},\mathbf{Y},\boldsymbol{p})$, $-L_{\mu,\lambda}(\mathbf{X},\mathbf{Y},\boldsymbol{p})$ serves as the lower bound for the objective function of (22). In Fig. 3, we see that Algorithm 3 needs more running time to converge compared with Algorithm 2, both $L_{\mu,\lambda}(\mathbf{X},\mathbf{Y},\boldsymbol{p})$ and γ converges in about 6 seconds when $M = 6$, and about 30 seconds when $M = 12$. As seen, $-L_{\mu,\lambda}(\mathbf{X},\mathbf{Y},\boldsymbol{p})$ is monotonically increasing until the algorithm converges, and the approximation gap between $-L_{\mu,\lambda}(\mathbf{X},\mathbf{Y},\boldsymbol{p})$ and γ increases as the UAV's number changes from 6 to 12. The convergence results of Fig. 2 and Fig. 3 imply that the algorithms running times are greatly affected by the UAV's number, for large numbers of UAVs, we can divide the UAVs and available RBs into multiple small scale parts, thus each independent part can be efficiently optimized by the proposed methods.

B. SYSTEM PERFORMANCE

The system performance of the proposed algorithms is evaluated in this subsection. We start by analyzing the effect of the exponential coefficient n which is introduced in (22), then we study the simulation results of a typical example, followed by the performance comparison of different methods.

1) IMPACT OF EXPONENTIAL COEFFICIENT n

As discussed in Section IV, n is a key factor for the relaxation of the problem (13). We investigate the relationship between the ultimate minimum SINR levels of UAVs and the exponential coefficient n with Algorithm 3, the averaged results by multiple independent running are illustrated in Fig. 4. For $n = 1$, problem (22) is exactly (13), and the corresponding system performance is the poorest as expected; for $n > 1$, the system performance is significantly improved. In addition, the exponential coefficient n should not be chosen too large to avoid the stringent conditioning property of the optimization problem. As seen from Fig. 4, the system performance keeps stable for $2 \le n \le 8$, and begins to decrease slightly when $n > 8$. For simulations, the exponential coefficient is simply taken as $n = 6$ in the following.

2) A SIMULATION EXAMPLE

In this example, we study a typical case and present the detailed optimization results in Fig. 5, the simulation settings are basically the same as before, i.e., $M = 6, N = 5, J = 5$. We randomly generate the UAVs' initial coordinates and their flying velocity vectors, the corresponding location dependent channel gain $\{C_k^j\}_{k\in\mathcal{M},j\in\mathcal{J}}$ between each UAV and the BS is drawn in Fig. 5a, in which the dark blue slots for UAV 2 and 3 are caused by the NLoS attenuation. In Algorithm 2 and Algorithm 3, we refer to the steps for updating $\mathbf{X}$ and $\mathbf{Y}$ as Stage I, and Stage II refers to the steps for updating $\boldsymbol{p}$. Through Stage I with Algorithm 3, the RBs assignment pattern is obtained as shown in Fig. 5b, and the corresponding SINR level of each UAV is depicted in Fig. 5c. We see that

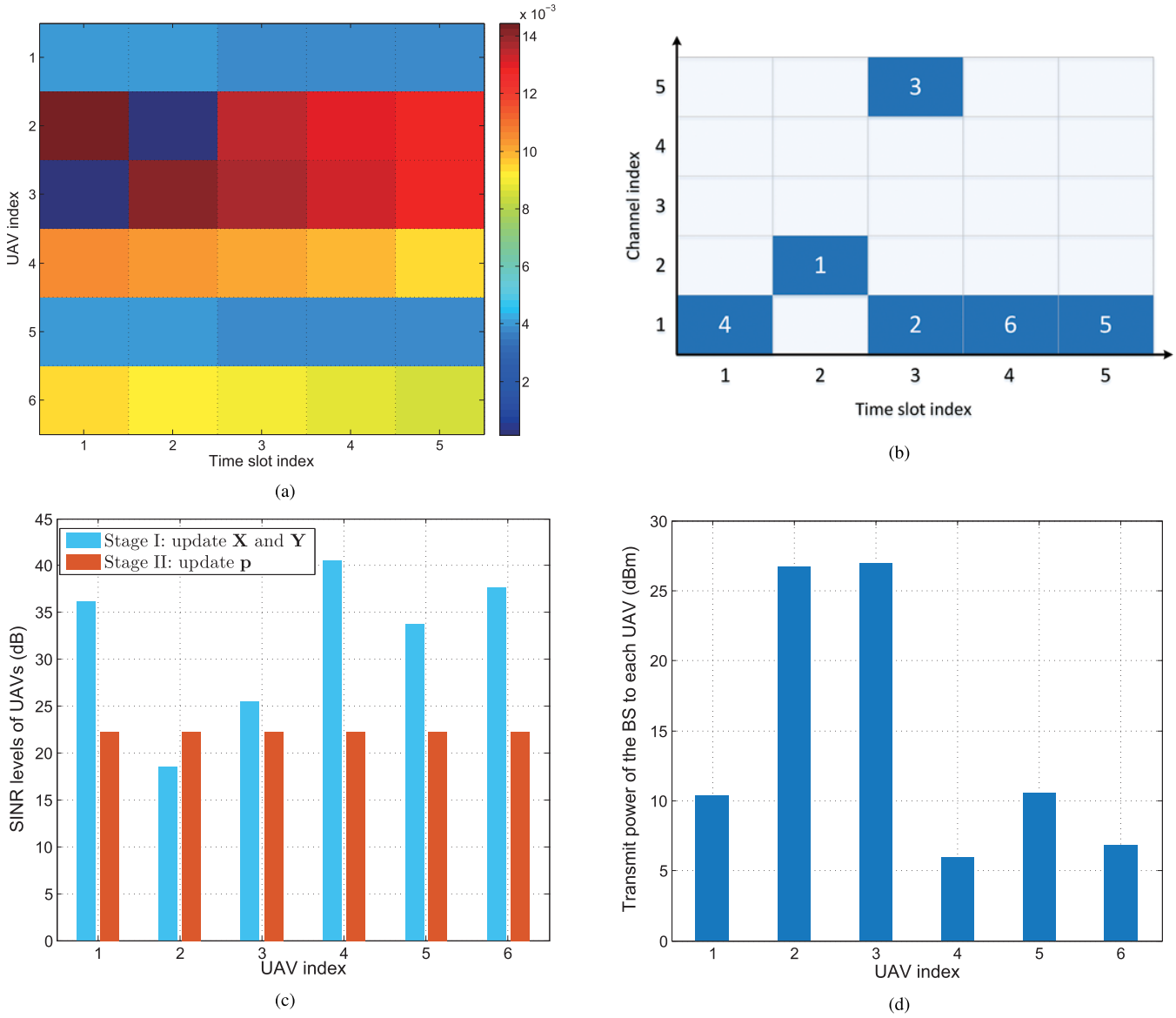

FIGURE 5. The simulation results for an example ($M = 6, N = 5, J = 5$). (a) Location dependent channel gain. (b) RBs assignment for UAVs. (c) SINR levels of UAVs. (d) Transmit power of the BS to each UAV.

the lowest SINR level is among UAV 2 and 3, both of whom receive the control signal at slot 3. Except for the transmit power of the BS, the SINR level of each UAV is determined by its channel gain and the mutual ACI. Therefore, on one hand, the UAVs should avoid occupying the NLoS attenuated time slots; on the other hand, for UAVs which are receiving control signal simultaneously, the interval between their occupying channels should be as large as possible. In addition, since we have considered a fairness objective in the optimization problem, thus in the RBs assignment results, the two UAVs 2 and 3 who experience the best channel gains, are assigned to the same time slot. In Stage II, the transmit power of the BS to the UAVs are further optimized, it observes from Fig. 5c that the SINR levels of all UAVs are reaching to a consistent level (i.e. 22.26 dB), and the lowest SINR level is promoted about 19.87% compared with Stage I. Fig. 5d shows the resulting transmit power of the BS to each UAV, which implies that the BS tends to allocate more power to the UAVs which have received lower SINR levels in Stage I, and vice versa.

3) PERFORMANCE COMPARISONS

To examine the performance of the proposed methods, we evaluate them under different scenario characterizations. Since there are no existing proposed schemes can apply to our problem, for a clear viewpoint of the performance gain brought by the proposed optimization algorithms, we also propose a baseline scheme as the benchmark. The base-

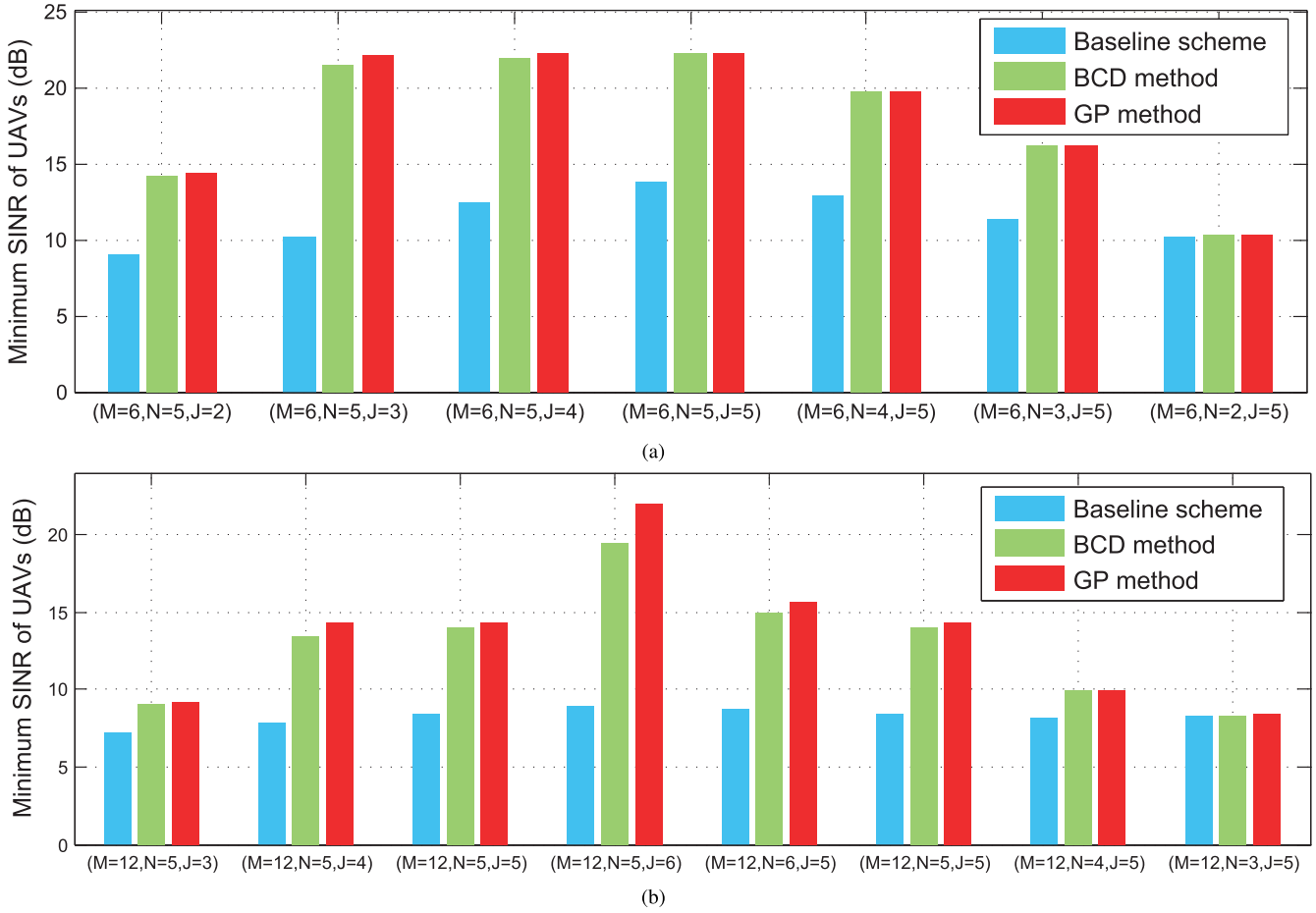

FIGURE 6. System performance under different scenario characterizations.

line scheme consists of two steps, the first step is to randomly assign each UAV a RB, while in the second step, with the fixed RBs assignment we optimize the BS's transmit power by the eigenvalue decomposition method. For a fairer comparison, the three methods are implemented under the same realization of the scenario. Since that the optimal performance of the considered optimization problem can hardly be determined within an acceptable time, we run Algorithm 3 multiple times with the random initial points and choose the best result as the upper bound performance. The results of the baseline scheme and the BCD-based method are averaged by multiple independent running. From Fig. 6, it can be observed that there is a large gap of the system performance between the baseline scheme and the upper bound by GP-based method. The BCD-based method offers superior performance over the baseline scheme, and its averaged results are close to the upper bound performance.

VII. CONCLUSIONS

In this paper, we investigated the reliable control signal reception of multiple UAVs in the presence of adjacent channel interference. Specifically, to improve the SINR levels of UAVs' control signal, we formulated a max-min-fairness optimization problem which jointly considered the optimization of time-frequency RBs scheduling and BS transmit power allocation. Such a problem contains the subscript optimization variables, which is difficult to process. To tackle this challenge, we equivalently transformed this problem into a more tractable form, then we utilized the rank-one property to further transform the problem into an equivalent but more simple formulation. Next, to solve the considered problem, we developed two efficient methods–namely, the block coordinate descent based method and the gradient projection based method. Furthermore, Simulation results showed the convergence properties of proposed algorithms, and the comparison results demonstrated the superiority of the proposed design.

REFERENCES

[1] S. Chandrasekharan *et al.*, "Designing and implementing future aerial communication networks," *IEEE Commun. Mag.*, vol. 54, no. 5, pp. 26–34, May 2016.

[2] M. Tortonesi, C. Stefanelli, E. Benvegnu, K. Ford, N. Suri, and M. Linderman, "Multiple-UAV coordination and communications in tactical edge networks," *IEEE Commun. Mag.*, vol. 50, no. 10, pp. 48–55, Oct. 2012.

[3] H. Wang, G. Ding, F. Gao, J. Chen, J. Wang, and L. Wang, "Power control in UAV-supported ultra dense networks: Communications, caching, and energy transfer," *IEEE Commun. Mag.*, to be published.
[4] M. Mozaffari, W. Saad, M. Bennis, and M. Debbah, "Unmanned aerial vehicle with underlaid device-to-device communications: Performance and tradeoffs," *IEEE Trans. Wireless Commun.*, vol. 15, no. 6, pp. 3949–3963, Jun. 2016.
[5] Y. Zeng, R. Zhang, and T. J. Lim, "Wireless communications with unmanned aerial vehicles: Opportunities and challenges," *IEEE Commun. Mag.*, vol. 54, no. 5, pp. 36–42, May 2016.
[6] Q. Feng, E. K. Tameh, A. R. Nix, and J. Mcgeehan, "WLCp2-06: Modelling the likelihood of line-of-sight for air-to-ground radio propagation in urban environments," in *Proc. IEEE Global Commun. Conf (GLOBECOM)*, San Francisco, CA, USA, Nov./Dec. 2006, pp. 1–5.
[7] A. Al-Hourani, S. Kandeepan, and A. Jamalipour, "Modeling air-to-ground path loss for low altitude platforms in urban environments," in *Proc. IEEE Global Commun. Conf (GLOBECOM)*, Austin, TX, USA, Dec. 2014, pp. 2898–2904.
[8] M. Mozaffari, W. Saad, M. Bennis, and M. Debbah, "Drone small cells in the clouds: Design, deployment and performance analysis," in *Proc. IEEE Global Commun. Conf (GLOBECOM)*, San Diego, CA, USA, Sep. 2015, pp. 1–6.
[9] C. Zhang and W. Zhang, "Spectrum sharing for drone networks," *IEEE J. Sel. Areas Commun.*, vol. 35, no. 1, pp. 136–144, Jan. 2017.
[10] M. Mozaffari, W. Saad, M. Bennis, and M. Debbah. (Apr. 2017). "Wireless communication using unmanned aerial vehicles (UAVs): Optimal transport theory for hover time optimization." [Online]. Available: https://arxiv.org/abs/1704.04813
[11] H. Nagarajan, S. Rathinam, and S. Darbha, "Synthesizing robust communication networks for unmanned aerial vehicles with resource constraints," *J. Dyn. Sys., Meas., Control*, vol. 137, no. 6, p. 061001, 2015.
[12] A. Al-Hourani, S. Kandeepan, and S. Lardner, "Optimal LAP altitude for maximum coverage," *IEEE Wireless Commun. Lett.*, vol. 3, no. 6, pp. 569–572, Dec. 2014.
[13] Y. Zeng, R. Zhang, and T. J. Lim, "Throughput maximization for UAV-enabled mobile relaying systems," *IEEE Trans. Commun.*, vol. 64, no. 12, pp. 4983–4996, Dec. 2016.
[14] M. Mozaffari, W. Saad, M. Bennis, and M. Debbah. (Sep. 2017). "Mobile unmanned aerial vehicles (UAVs) for energy-efficient Internet of Things communications." [Online]. Available: https://arxiv.org/abs/1703.05401
[15] Q. Wu, Y. Zeng, and R. Zhang. (May 2017). "UAV-enabled aerial base station (BS) I/III: Joint trajectory and communication design for multi-UAV enabled wireless networks." [Online]. Available: https://arxiv.org/abs/1705.02723
[16] T. S. Rappaport, *Wireless Communications: Principles and Practice*. Englewood Cliffs, NJ, USA: Prentice-Hall, 1996.
[17] M. Kim, Y. Han, Y. Yoon, Y.-J. Chong, and H. Lee, "Modeling of adjacent channel interference in heterogeneous wireless networks," *IEEE Commun. Lett.*, vol. 17, no. 9, pp. 1774–1777, Sep. 2013.
[18] W. Yang and G. Xu, "Optimal downlink power assignment for smart antenna systems," in *Proc. IEEE Int. Conf. Acoust., Speech Signal Process. (ICASSP)*, Seattle, WA, USA, May 1998, pp. 3337–3340.
[19] S. P. Boyd and L. Vandenberghe, *Convex Optimization*. Cambridge, U.K.: Cambridge Univ. Press, 2004.
[20] W. Wang and M. Á. Carreira-Perpiñán. (Sep. 2013). "Projection onto the probability simplex: An efficient algorithm with a simple proof, and an application." [Online]. Available: https://arxiv.org/abs/1309.1541
[21] M. Grant and S. Boyd. (Sep. 2013). *CVX: Matlab Software for Disciplined Convex Programming, Version 2.0 beta*. [Online]. Available: http://cvxr.com/cvx
[22] J. Nocedal and S. J. Wright, *Numerical Optimization*. New York, NY, USA: Springer, 2006.
[23] H. H. M. Tam, H. D. Tuan, D. T. Ngo, T. Q. Duong, and H. V. Poor, "Joint load balancing and interference management for small-cell heterogeneous networks with limited backhaul capacity," *IEEE Trans. Wireless Commun.*, vol. 16, no. 2, pp. 872–884, Feb. 2016.
[24] M. Pischella, R. Zakaria, and D. Le Ruyet, "Resource block-level power allocation in asynchronous multi-carrier D2D communications," *IEEE Commun. Lett.*, vol. 21, no. 4, pp. 813–816, Apr. 2017.

ZHEN XUE received the B.S. degree in electrical engineering from Xidian University, Xi'an, China, in 2012, and the M.S. degree in information and communication engineering form the College of Communications Engineering, Nanjing, China, in 2015. He is currently pursuing the Ph.D. degree with the College of Communications Engineering. His research interests focus on cognitive radio networks resource optimization, machine learning, and big spectrum data analytics for future wireless networks.

JINLONG WANG (AM'98–M'09–SM'13) received the B.S. degree in wireless communications, the M.S. degree, and the Ph.D. degree in communications and electronic systems from the Institute of Communications Engineering, Nanjing, China, in 1983, 1986, and 1992, respectively. He is currently a Professor with the Army Engineering University of PLA, Nanjing. He has published widely in the areas of signal processing for wireless communications and networking. His current research interests include soft-defined radio, cognitive radio, and green wireless communication systems. He was a Co-Chair of the IEEE Nanjing Section.

QINGJIANG SHI received the B.S. degree in electronic engineering from the China University of Petroleum, Dongying, China, in 2003, and the Ph.D. degree in communication engineering from Shanghai Jiao Tong University, Shanghai, China, in 2011. From 2009 to 2010, he visited the Prof. Z.-Q. (Tom) Luos Research Group, University of Minnesota, Twin Cities. In 2011, he was a Research Scientist at the Research and Innovation Center (Bell Labs China), Alcatel-Lucent Shanghai Bell Company Ltd., China. He is currently a Professor with the College of Electronic and Information Engineering, Nanjing University of Aeronautics and Astronautics, Nanjing, China. His current research interests lie in algorithm design for signal processing in advanced MIMO, cooperative communication, physical layer security, energy-efficient communication, wireless information, and power transfer. He has served as a TPC member for IEEE Globecom/ICC from 2012 to 2013, and a peer reviewer for a variety of IEEE journals and conferences.

He received the Nomination Award of National Excellent Doctoral Dissertation of China in 2013, the Shanghai Excellent Doctoral Dissertation Award in 2012, and the Best Paper Award from the IEEE PIMRC'09 Conference.

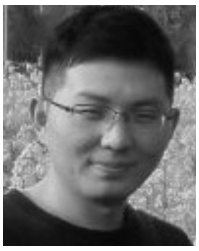

GUORU DING (S'10–M'14–SM'16) received the B.S. degree (Hons.) in electrical engineering from Xidian University, Xi'an, China, in 2008, and the Ph.D. degree (Hons.) in communications and information systems form the College of Communications Engineering, Nanjing, China, in 2014. Since 2014, he has been an Assistant Professor with the College of Communications Engineering and a Research Fellow at the National High Frequency Communications Research Center, China. Since 2015, he has been a Post-Doctoral Research Associate with the National Mobile Communications Research Laboratory, Southeast University, Nanjing. His research interests include cognitive radio networks, massive MIMO, machine learning, and big data analytics over wireless networks.

Dr. Ding has acted as a Technical Program Committees member for a number of international conferences, including the IEEE Global Communications Conference, the IEEE International Conference on Communications, and the IEEE Vehicular Technology Conference. He is a Voting Member of the IEEE 1900.6 Standard Association Working Group. He was a recipient of the Best Paper Awards from EAI MLICOM 2016, IEEE VTC 2014-Fall, and IEEE WCSP 2009. He received the Alexander von Humboldt Fellowship in 2017 and the Excellent Doctoral Thesis Award of China Institute of Communications in 2016. He has served as a Guest Editor for the IEEE JOURNAL ON SELECTED AREAS IN COMMUNICATIONS (special issue on spectrum sharing and aggregation in future wireless networks). He is currently an Associate Editor of the *Journal of Communications and Information Networks*, the *KSII Transactions on Internet and Information Systems,* and the *AEÜ-International Journal of Electronics and Communications*.

QIHUI WU (SM'13) received the B.S. degree in communications engineering, and the M.S. degree and the Ph.D. degree in communications and information systems from the Institute of Communications Engineering, Nanjing, China, in 1994, 1997, and 2000, respectively. From 2003 to 2005, he was a Post-Doctoral Research Associate with Southeast University, Nanjing. From 2005 to 2007, he was an Associate Professor with the College of Communications Engineering, PLA University of Science and Technology, Nanjing, where he served as a Full Professor from 2008 to 2016. In 2011, he was an Advanced Visiting Scholar with the Stevens Institute of Technology, Hoboken, NJ, USA. Since 2016, he has been a Full Professor with the College of Electronic and Information Engineering, Nanjing University of Aeronautics and Astronautics, Nanjing. His current research interests span the areas of wireless communications and statistical signal processing, with emphasis on the system design of software-defined radio, cognitive radio, and smart radio.